Contrib Mineral Petrol (2000) 138: 249–264

Peter W. Reiners · Paul E. Hammond
Juliet M. McKenna · Robert A. Duncan

Young basalts of the central Washington Cascades, flux melting of the mantle, and trace element signatures of primary arc magmas

Received: 2 March 1999 / Accepted: 18 August 1999

Abstract Basaltic lavas from the Three Sisters and Dalles Lakes were erupted from two isolated vents in the central Washington Cascades at 370–400 ka and 2.2 Ma, respectively, and have distinct trace element compositions that exemplify an important and poorly understood feature of arc basalts. The Three Sisters lavas are calc-alkaline basalts (CAB) with trace element compositions typical of most arc magmas: high ratios of large-ion-lithophile to high-field-strength elements (LILE/HFSE), and strong negative Nb and Ta anomalies. In contrast, the Dalles Lakes lavas have relatively low LILE/HFSE and no Nb or Ta anomalies, similar to ocean-island basalts (OIB). Nearly all Washington Cascade basalts with high to moderate incompatible element concentrations show this CAB or OIB-like compositional distinction, and there is pronounced divergence between the two magma types with a large compositional gap between them. We show that this trace element distinction can be easily explained by a simple model of flux-melting of the mantle wedge by a fluid-rich subduction component (SC), in which the degree of melting (F) of the peridotite source is correlated with the amount of SC added to it. Distinctive CAB and OIB-like trace element compositions are best explained by a flux-melting model in which dF/dSC decreases with increasing F, consistent with isenthalpic (heat-balanced) melting. In the context of this model, CAB trace element signatures simply reflect large degrees of melting of strongly SC-fluxed peridotite along relatively low dF/dSC melting trends, consistent with derivation from relatively cold mantle. Under other conditions (i.e., small degrees of melting or large degrees of melting of weakly SC-fluxed peridotite [high dF/dSC]), either OIB- or MORB (mid-ocean ridge basalt)-like compositions are produced. Trace element and isotopic compositions of Washington Cascade basalts are easily modeled by a correlation between SC and F across a range of mantle temperatures. This implies that the dominant cause of arc magmatism in this region is flux melting of the mantle wedge.

P.W. Reiners (✉)[1]
Division of Geological and Planetary Sciences,
MS 100-23, California Institute of Technology,
Pasadena, CA 91125, USA
e-mail: reiners@wsu.edu

P.E. Hammond
Department of Geology, Portland State University,
Portland, OR 97207, USA

J.M. McKenna
Montgomery Watson Americas, Inc., Pasadena, CA 91101, USA

R.A. Duncan
College of Oceanic and Atmospheric Sciences,
Oregon State University, Corvallis,
OR 97331, USA

Present address:
[1] Department of Geology, Washington State University, Pullman, WA 99164, USA

Editorial responsibility: T.L. Grove

Introduction

Arc basalts are typically enriched in LILE and other fluid mobile elements (e.g., Cs, Rb, Ba, Sr, K, U, Th, LREE) relative to most HFSE (especially Nb and Ta, and to lesser degrees Hf, Zr, and Ti). This characteristic is generally thought to be caused by addition of a LILE-rich fluid or melt derived from a subducted slab to a mantle wedge source (e.g., Gill 1981; Tatsumi et al. 1986; Hawkesworth et al. 1993, 1994; Stolper and Newman 1994). Basalts displaying such trace element features are commonly termed CAB (e.g., Leeman et al. 1990; Conrey et al. 1997; Bacon et al. 1997). Many arc basalts, however, especially in the Cascades, have relatively high incompatible element concentrations but do not have high LILE/HFSE or negative Nb and Ta anomalies. Because these trace element characteristics are common to many ocean-island basalts, these have been termed intraplate-, or OIB-like basalts (e.g., Luhr et al. 1989, Luhr 1997; Leeman et al. 1990; Conrey et al. 1997; Bacon et al. 1997;

Márquez et al. 1999), even though the arc in which they are found may have no obvious connection to intraplate- or plume-related tectonic settings or processes.

Here we report age and chemical results from young lavas of two small basaltic fields in the central Washington Cascades that clearly exemplify the CAB-OIB compositional distinction. We show that this distinction cannot be explained simply by different amounts of fluid-rich subduction component (SC) from the subducting slab in each mantle source. However, the distinct and divergent CAB-OIB array is easily modeled as flux-melting of the mantle, involving a correlation between the amount of SC added to the mantle source and the degree of melting of the source. One important implication of this modeling is that OIB-like arc basalts can be produced by the same melting process and from the same mantle source as CAB melts, simply by relatively low-degrees of melting of a mantle region that has had a comparatively small amount of slab component added to it. Thus, OIB-like trace element compositions do not necessarily indicate the presence of plume material or ocean-island-like melting processes under arcs.

Samples and methods

The Three Sisters (TS) and Dalles Lakes (DL) basalts were erupted from relatively small and presumably short-lived vents about 30 km north of Mt. Rainier (Fig. 1). Our mapping, as well as earlier work (Fischer 1970; Hartman 1973; Hammond 1980), indicates that the TS and DL basalts were erupted subaerially through older andesitic porphyry and volcaniclastic deposits. Each vent produced approximately 4–10 lava flows with a similar phenocryst content of olivine, and rare plagioclase and/or clinopyroxene. The TS and DL basalts are the only known volcanic rocks of the High Cascades (late Cenozoic to recent) between Mt. Rainier and Glacier Peak (Hammond 1980; Luedke and Smith 1982), a distance of nearly 150 km. Their apparently primitive compositions provide insights into primary magma compositions and mantle-melting processes in this part of the Cascade arc.

We collected and analyzed 7 TS and 11 DL samples for major- and trace-element compositions (Table 1). Analyses were performed at Washington State University and CHEMEX Labs (Vancouver, B.C.) using standard XRF methods for major elements and ICP-MS for trace elements. Three (including two flows and one dike) TS samples and one DL flow sample were dated by whole-rock, single-step, total-fusion $^{40}Ar/^{39}Ar$ methods, and one TS sample was also dated by incremental heating $^{40}Ar/^{39}Ar$ methods, at Oregon State University.

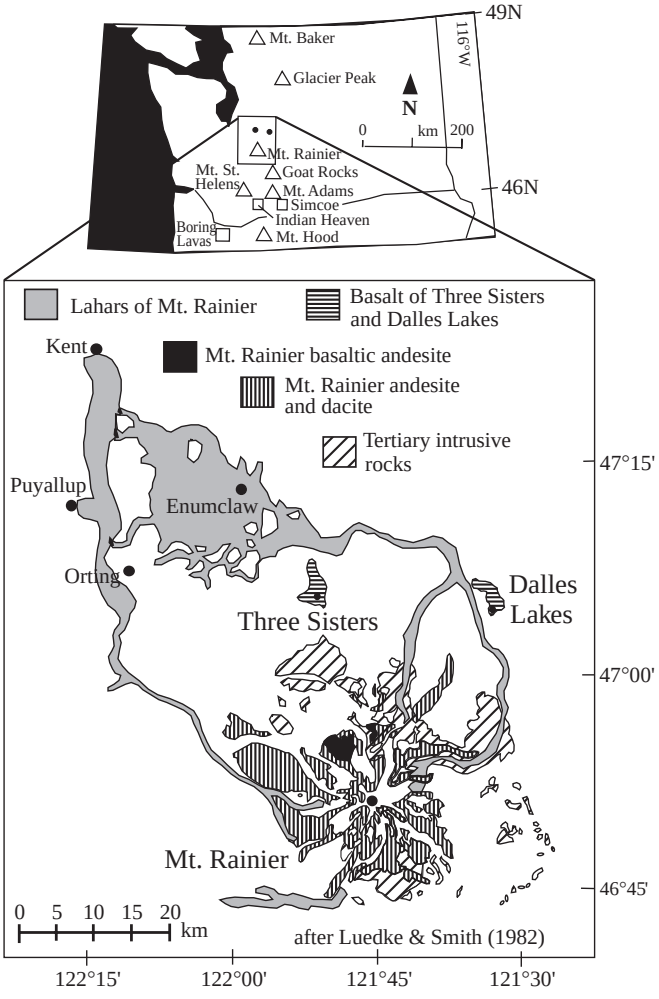

Fig. 1 Generalized geologic map of the central Washington Cascades near Mt. Rainier (after Luedke and Smith 1982; Hammond 1998) showing the locations and approximate areal distribution of the Three Sisters and Dalles Lakes basalts. Shown in the *inset* are the locations of other Washington and northern Oregon volcanoes (*triangles*) and selected volcanic fields discussed in this paper (*squares*). The Three Sisters and Dalles Lakes basalts were originally described by Fischer (1970) and Hartman (1973), who named them the Basalts of Canyon Creek and Dalles Ridge, respectively. For stratigraphic clarity (because of the abundance of "Canyon Creek" names in the Cascades, and because we reserve the name "Dalles Ridge" for one of the thick, older volcanic units that composes most of the ridges in the area) we suggest the new names

Results

$^{40}Ar/^{39}Ar$ ages indicate that the Dalles Lakes basalt was erupted at 2.2 ± 0.05 (1σ) Ma, and is significantly older than the Three Sisters basalt (Table 1). Single-step fusion ages for two samples (365 ± 50 and 385 ± 71 ka) and plateau and isochron ages of one sample (398 ± 15 and 377 ± 42 ka, respectively) indicate an age of about 370–400 ka for the Three Sisters (Table 1). The single-step fusion procedure of 96PRTS6 produced a very low radiogenic Ar yield and large analytical uncertainty that precludes confident age assignment, but it is concordant with the results of the other samples.

High MgO (8–10 wt%), Mg#(60–70), and compatible trace element contents indicate that the DL and TS lavas are primitive basalts that have experienced little

Table 1 $^{40}Ar/^{39}Ar$ ages (Ma) of samples of the Dalles Lakes and Three Sisters basalts, central Washington Cascades. ±are 1σ

	96PRDR2	96PRTS1	96PRTS6	96PRTS11
Single-step, total fusion age	2.18 ± 0.05	0.385 ± 0.071	0.271 ± 0.174	0.365 ± 0.050
Radiogenic Ar	89.1%	38.3%	1.30%	74.1%
Plateau (2 steps, 80% of gas)				0.398 ± 0.015
Isochron (5 steps)				0.377 ± 0.042

fractional crystallization (Tables 2, 3). In many other respects, however, major- and trace-element compositions of DL and TS lavas are distinct: DL lavas are alkalic basalt whereas TS lavas are subalkalic basalts and basaltic andesites (Fig. 2). DL lavas also have high TiO_2 and Fe_2O_3, and low SiO_2 relative to the TS lavas (Fig. 2, Table 1). In detail, there are subtle but notable compositional variations among samples from each suite. In particular, most of the relatively high SiO_2 (>52.5%) TS samples show slightly different trace element trends than the rest of the TS suite, with higher Ni and incompatible element concentrations. DL lavas also show interesting intrasuite trends, particularly correlations between Ni and incompatible elements such as Ba, La, and Sr (Tables 2, 3). Overall, however, the most remarkable compositional distinctions are contrasting ratios of LILE and other fluid-mobile elements (e.g., Cs, Rb, Ba, Th, U, Sr), and HFSE (e.g.,

Table 2 Compositions of samples of the Dalles Lakes basalt, central Washington Cascades

	96PRDR2	PHA92262	PHA92264	PHA92265	PHA92266	PHA92267	PHA92268
SiO_2	47.60	48.90	49.17	50.14	49.52	47.98	48.53
TiO_2	1.87	1.41	1.53	1.49	1.51	1.22	1.79
Al_2O_3	16.05	16.25	15.67	16.20	16.06	16.70	15.27
Fe_2O_3	10.6	11.52	10.68	11.34	11.34	12.21	10.17
CaO	8.19	8.88	8.69	8.85	8.74	9.06	8.38
MgO	8.06	8.01	8.37	8.07	8.13	9.03	8.3
MnO	0.16	0.16	0.16	0.16	0.16	0.18	0.15
K_2O	1.23	0.70	0.91	0.83	0.82	0.35	1.23
Na_2O	3.22	3.49	3.56	3.76	3.47	3.12	3.59
P_2O_5	0.44	0.31	0.32	0.29	0.29	0.17	0.44
LOI	0.90						
Total	98.37	99.63	99.06	101.13	100.04	100.02	97.85
Ba	359	171	207	170	192	94	297
Ce	55	34	45	39	28	29	56
Cs	0.3						
Co	44.5						
Cr	342	267	273	265	270	247	270
Cu	45	33	52	53	48	17	42
Dy	4.7						
Er	2.4						
Eu	1.8						
Gd	5.4						
Ga	20	20	18	16	18	14	18
Hf	4						
Ho	0.9						
La	25	3	13	6	11	22	21
Lu	0.3						
Nd	26						
Ni	195	139	153	144	147	135	162
Nb	29	16.6	21.4	17.8	19.5	8.3	31.9
Pr	7.1						
Rb	20	6	14	14	12	6	19
Sc		29	28	28	32	36	30
Sm	5.7						
Sr	589	396	457	422	421	302	574
Ta	2.5						
Tb	0.9						
Th	2		2	2			3
Tm	0.4						
U	0.5						
V	175	178	182	176	185	179	181
Yb	2.6						
Y	24	24	23	24	24	24	23
Zn	90	89	87	88	87	82	82
Zr	187	131	153	140	144	100	191

Table 3 Compositions of samples of the Three Sisters basalt, central Washington Cascades

	96PRTS1	96PRTS6	96PRTS11	PHA97057	PHA97058	PHA97059	PHA97060	PHA97061	PHA97062	PHA97064	PHA97065
SiO_2	50.98	50.56	52.51	52.60	52.38	51.93	50.12	50.78	53.32	53.53	54.42
TiO_2	1.15	1.09	1.25	1.15	1.12	1.18	1.19	1.17	1.16	1.18	1.26
Al_2O_3	15.67	15.55	15.34	16.35	15.80	16.36	16.58	16.63	15.61	15.83	15.56
Fe_2O_3	9.85	9.36	8.90	9.29	9.17	9.47	10.16	9.78	8.55	8.32	7.99
CaO	8.70	8.33	7.65	8.70	8.90	8.41	8.23	8.81	7.67	7.75	7.61
MgO	8.83	9.57	9.07	8.22	8.19	8.36	9.94	9.23	9.05	8.64	8.54
MnO	0.14	0.14	0.13	0.14	0.14	0.15	0.16	0.15	0.13	0.13	0.12
K_2O	1.2	1.02	1.43	1.16	1.19	1.26	0.71	0.91	1.35	1.37	1.45
Na_2O	2.9	2.82	3.21	3.2	3.19	3.07	2.73	3.01	3.43	3.49	3.65
P_2O_5	0.29	0.28	0.36	0.30	0.29	0.30	0.25	0.30	0.33	0.35	0.36
LOI	0.39	0.51	0.0								
Total	100.15	99.3	99.92	101.11	100.37	100.49	100.06	100.76	100.60	100.60	100.96
Ba	369	360	450	348	350	353	297	379	364	396	407
Ce	55.5	56	59.5	58	63	71	42	62	68	66	57
Cs	0.5	0.6	1.1								
Co	41	41.5	38								
Cr	411	479	479	314	309	332	392	356	388	359	372
Cu	20	30	35	6	9	2	13	7	15	25	16
Dy	4.2	3.7	3.5								
Er	2.5	2.4	2.1								
Eu	1.6	1.6	1.6								
Gd	4.3	4.6	4.5								
Ga	19	20	20	21	17	19	21	16	19	17	21
Hf	5	4	4								
Ho	0.8	0.8	0.8								
La	23	24.5	26	26	23	28	35	23	26	24	20
Lu	0.4	0.4	0.3								
Nd	27	26.5	27.5								
Ni	85	130	190	52	54	64	94	58	185	158	168
Nb	7	8	13	6.9	7.1	7.9	8.3	7	11.8	11.1	13.7
Pr	7.3	7.5	7.9								
Rb	22	17.6	30.8	20	19	21	15	6	24	20	26
Sc				29	30	30	27	31	24	22	20
Sm	5.3	5.2	6.1								
Sr	728	718	763	720	743	711	598	787	752	809	762
Ta	0.5	0.5	1.0								
Tb	0.7	0.7	0.7								
Th	3	4	4	2	5	5	6	7	5	9	7
Tm	0.4	0.4	0.2								
U	1.0	1.5	1.5								
V	150	135	135	182	169	171	176	181	164	167	181
Yb	2.3	2.1	1.8								
Y	22.5	21.5	19.5	22	23	23	25	24	20	20	19
Zn	70	75	90	73	72	82	83	74	72	72	77
Zr	166	150	157	176	177	178	172	187	173	174	178

Nb, Ta, Zr, Ti). These differences are evident in spider diagrams, which show that the TS lavas have strong negative Nb and Ta (and to a lesser degree Ti) anomalies, whereas the DL lavas do not (Fig. 3).

Strongly contrasting LILE/HFSE compositions distinguish not only the DL and TS basalts but also many basalts from the southern Washington Cascades (Fig. 4), and have been used to define two distinct types of primary magmas (Leeman et al. 1990; Bacon et al. 1997; Conrey et al. 1997). High LILE/HFSE and negative Nb and Ta anomalies of the TS lavas are typical of what is often called the arc basalt, or CAB. CAB lavas, including many from Indian Heaven, Mt. Rainier, Mt. Adams, and scattered localities in southern Washington and northern Oregon (Fig. 4), are typified by low HFSE (e.g., <20 ppm Nb), and variable but generally high LILE contents that are not correlated with Nb content. These lavas also have generally high Ba, Th, Ba/Nb, and Ba/Zr, and low Nb/Zr. They also typically have relatively high Cs/K, La/Nb, SiO_2, and K_2O, and low Fe_2O_3 and TiO_2 (Leeman et al. 1990; Bacon et al. 1997; Conrey et al. 1997).

A clearly separate group of basalts, consisting of DL and other OIB-like lavas is best characterized by a wide range of HFSE, which is well correlated with LILE content, although LILE are generally at lower concentrations (for a given HFSE concentration, e.g., Fig. 4). The OIB-like lavas also have low Ba/Nb and a wide range of Nb/Zr, correlated with Ba/Zr. These have been termed intraplate, or OIB (Leeman et al. 1990; Bacon et al. 1997; Conrey et al. 1997). Besides Dalles Lakes, these lavas are common on Mt. St. Helens, Simcoe, and Mt. Adams.

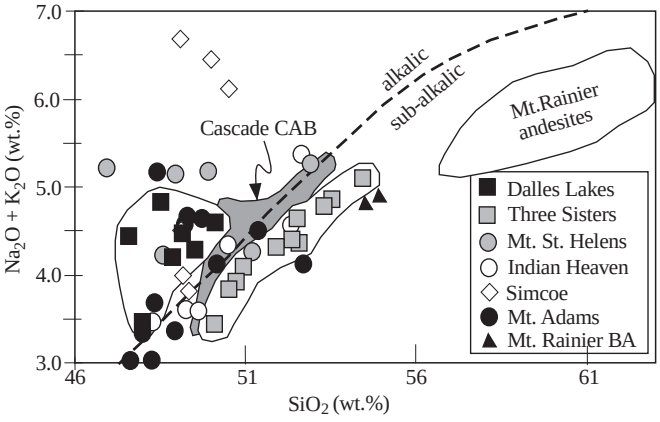

Fig. 2 Total alkalis (Na_2O + K_2O) versus SiO_2 (wt%). Data from volcanoes in central and southern Washington other than Three Sisters (*TS*) and Dalles Lakes (*DL*) are from Leeman et al. (1990), Conrey et al. (1997), Bacon et al. (1997), and McKenna (1994). Cascade CAB field includes samples in Conrey et al. (1997) classified as either CAB or high-K CAB. Alkalic-subalkalic basalt dividing line is from Miyashiro (1978)

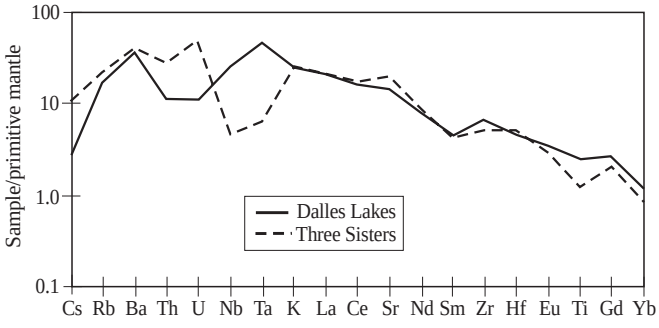

Fig. 3 Trace element compositions of DL sample 96PRDR2 and average of three TS samples (96PRTS1, 6, and 11), normalized to primitive mantle (Sun and McDonough 1989). Note enrichment of TS in Cs, Rb, Ba, Th, and U, and depletion in Nb, Ta, and Ti, relative to DL

Although not as obvious as the CAB and OIB-like basalts in Fig. 4, a third type of basalt, the low-K tholeiite, high-alumina olivine tholeiite, or MORB-like basalt, also occurs in the Cascades. MORB-like basalts typically have low incompatible element concentrations, falling near the origin in most of the plots in Fig. 4. The MORB-like basalts are found throughout the Cascades, and those plotted in Fig. 4 include the low Ba, Nb, and Th lavas from the Mt. Adams and Indian Heaven groups (Leeman et al. 1990; Bacon et al. 1997).

Discussion

The $^{40}Ar/^{39}Ar$ dates of the DL and TS basalts confirm the field-based suggestions of young eruption ages (Fischer 1970; Hartman 1973; Hammond 1980). They also demonstrate that late Cenozoic to recent volcanic activity in the central Cascades is not restricted to large stratovolcanoes and their immediate satellite vents. Both the ages and compositions of the TS and DL basalts make it unlikely that they are related to the magmatic system of Mt. Rainier. OIB-like trace element compositions of the DL basalts are unlike any known Rainier sample, and the 2.2 Ma age of the DL vent predates the earliest known Rainier eruption at about 500 ka (Sisson and Lanphere 1997). Although trace element compositions of the TS lavas are similar to those of the basaltic andesites at Echo and Observation Rocks, on the north side of Mt. Rainier (McKenna 1994), the TS lavas are more mafic (8–10 versus 6–7 wt% MgO), and much older than Echo and Observation Rocks (105 ka, from K/Ar dating by Lanphere and Sisson 1995).

Contrasting patterns of LILE and HFSE concentrations among the DL and TS basalts clearly exemplify the distinction between CAB and OIB-like lavas of the Cascades (Figs. 3, 4). At high or moderate concentrations of incompatible elements (e.g., high Ba/Nb or Nb/Zr), trace element differences between CAB and OIB-like lavas are not a matter of degree. There appears to be markedly distinct fields that diverge from a common region at low incompatible element concentrations (e.g., low Ba/Nb and low Nb/Zr). This distinct divergence of the CAB and OIB-like magmas and the lack of magmas with compositions intermediate between the two groups may provide an important constraint on sources and processes involved in arc magma genesis.

Trace element modeling

To investigate the potential significance of the distinct divergence of CAB and OIB-like compositions, we modeled the trace element effects of partial melting of peridotite mixed with (i.e. metasomatized by) varying amounts of a LILE-rich SC derived from a subducting slab. In most of our modeling we used a mantle peridotite composition and an SC composition (Fig. 5; Table 4) similar to those used in previous studies (Stolper and Newman 1994; Borg et al. 1997), but with some modifications. Abundances of several elements have been adjusted to provide good fits to flux-melting trends in trace element space, as presented below. In detail, the model peridotite composition we used in most of the model examples is slightly more enriched in incompatible elements than that of Stolper and Newman's (1994) and Borg et al.'s (1997) MORB source. However, the model peridotite is more depleted than Borg et al.'s OIB source, except for Nb and Ta, which are slightly more enriched (1.50 ppm Nb, 0.14 ppm Ta, compared with 1.13 and 0.10 ppm, respectively, in the OIB source). The positive Nb and Ta anomalies assumed for this peridotite source are consistent with positive Nb anomalies observed in unmetasomatized xenoliths from the continental lithospheric mantle in southern British Columbia (Sun and Kerrich, 1995), which may be similar to the mantle source under the Cascades.

Furthermore, Ionov and Hofmann (1995) showed that subcontinental mantle xenoliths with small modal

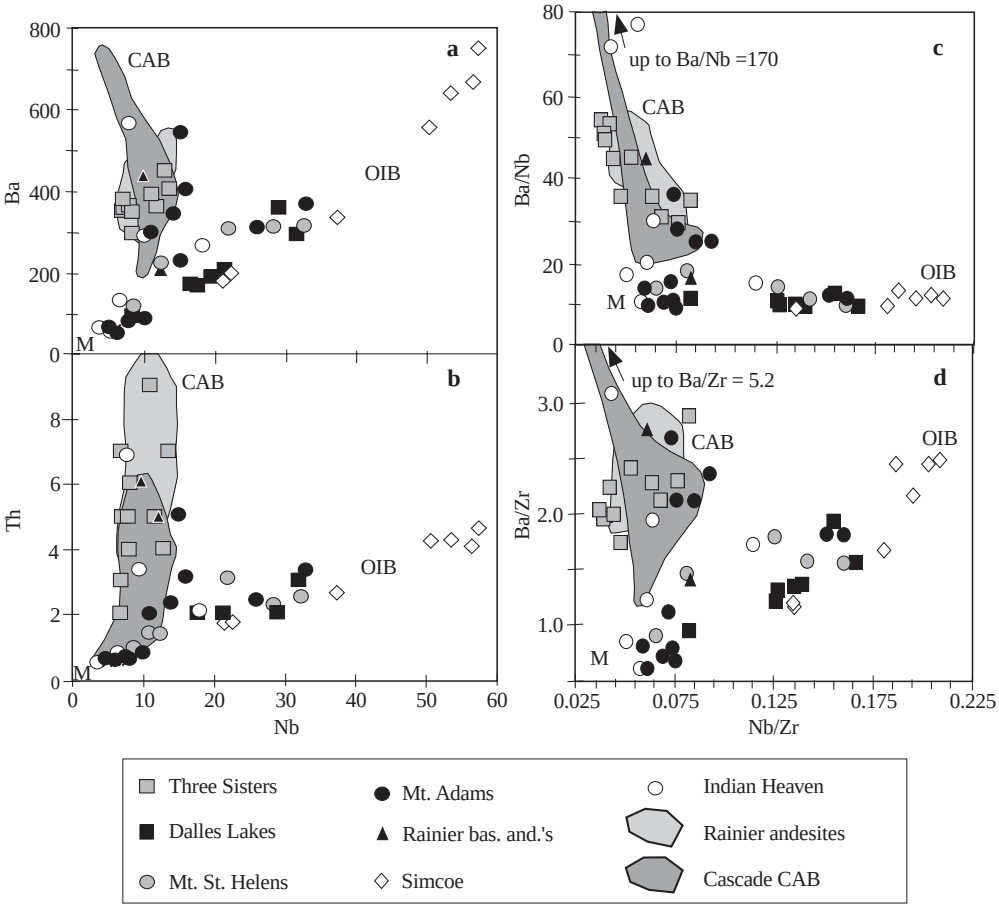

Fig. 4 Concentrations of, and ratios involving, LILE (Ba), Th, and HFSE (Nb, Zr) for the Three Sisters and Dalles Lakes basalts, as well as basalts from other areas in the central and southern Washington Cascades. CAB and OIB lavas form distinct and divergent trends in these plots, primarily caused by the low HFSE and high LILE/HFSE of CAB lavas. There is a paucity of lavas with intermediate compositions at moderate to high concentrations of incompatible elements. MORB-like basalts (near the region labeled *M*) have low concentrations of incompatible elements (and low Ba/Nb, Nb/Zr, and Ba/Zr) relative to CAB and OIB-like lavas. Data from sources listed in Fig. 2

Table 4 Peridotite and subduction component (SC) compositions used in model. Peridotite concentrations for Cs, Rb, U, K, La, Ce, Hf, and Yb are average of Borg et al. (1997) MORB and OIB sources. Other elements are adjusted to fit trends in Fig. 7, but are intermediate between Borg et al.'s MORB and OIB values (except for Nb and Ta). SC concentrations for La, Ce, and Sm are from Borg et al. (1997) (many of which are from Stolper and Newman 1994), other elements adjusted to fit trends, but are similar to those of Borg et al. (1997) and Stolper and Newman (1994)

	Peridotite	SC	Borg et al. MORB source	Borg et al. OIB source	Borg et al. SC
Cs	0.00465	3.5	0.0003	0.009	2
Rb	0.413	120	0.026	0.80	147
Ba	9	1500	0.288	13.1	1371
Th	0.07	16	0.0060	0.16	11
U	0.02	5.3	0.0025	0.028	4
Nb	1.5	8	0.12	1.13	46
Ta	0.14	0.5	0.0075	0.10	3
K	283.85	45,000	27.7	540	70,559
La	0.815	99	0.150	1.48	99
Ce	2.47	297	0.490	4.45	297
Sr	18	3500	5.77	28.7	4681
Nd	1.4	130	0.654	2.97	147
Sm	0.35	35	0.293	1.01	35
Zr	25	500	7.2	26.4	985
Hf	0.4	20	0.20	0.60	27
Eu	0.13	9	0.119	0.26	13
Ti	1000	30,000	996	1980	85,000
Gd	0.45	30	0.467	0.86	39
Yb	0.5	12	0.402	0.56	32

fractions (2–4%) of disseminated amphibole have almost identical Nb and Ta concentrations and very similar overall trace element patterns (Fig. 5). Peridotite with such trace element characteristics may dominate large regions of the mantle wedge under subduction zones. Although Borg et al. (1997) included amphibole in some

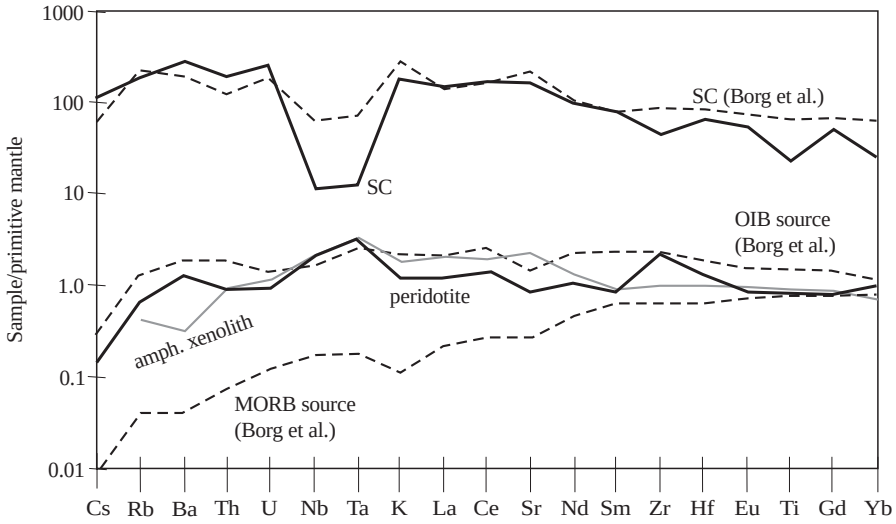

Fig. 5 Trace element compositions of peridotite and SC sources assumed in this study (*bold black lines*), compared with sources from Borg et al. (1997) (*dashed lines*), and a peridotite xenolith from the Siberian subcontinental mantle. (Ionov and Hofmann 1995)

of their models, our model peridotite does not contain amphibole, following the modeling of Stolper and Newman (1994), the thermodynamic models of Hirschmann et al. (1999), and the experimental results of Gaetani and Grove (1998). Pargasitic amphibole has been produced experimentally in spinel lherzolite in simulated metasomatic reactions (e.g., Sen and Dunn 1995), but experimental temperatures are generally subsolidus and much lower (950–1025 °C) than those assumed (>1225 °C) for the present study. Other experimental evidence (Dunn et al. 1993; Menner and Dunn 1995; Niida and Green 1999, and references therein) indicates that at pressures of 1–3 GPa amphibole breaks down or reacts completely out of the modal assemblage at relatively low temperatures near the solidus. For these reasons, we assume that at the relatively high degrees of melting required to reproduce magma compositions in our models (typically >5%), amphibole would not be a residual phase and would not affect the melt trace element patterns. Other trace element features of the DL and TS lavas, such as lack of negative Ba anomalies, also do not suggest significant amounts of residual amphibole.

The model SC composition that we use in most of the modeling (Fig. 5; Table 4) is very similar to that of Borg et al. (1997), which is the same as that of Stolper and Newman (1994) for all elements except those added by Borg et al.. There are, however, some differences. The most extreme differences are in the HFSE; the Nb, Ta, Zr, and Hf concentrations of this study are significantly more depleted (by factors of 1.3 to 6) than those in Borg et al.'s SC. The results of the flux melting models are not highly sensitive to the exact SC composition used, as long as it is strongly depleted in HFSE, which is widely believed to be an important chemical feature of slab-derived fluids (e.g., Gill 1981; Tatsumi et al. 1986; Hawkesworth 1993, 1994; Stolper and Newman 1994; Ayers et al.1997). The initial peridotite composition does, however, strongly influence trace element compositions of the melts. We show several important effects of varying both SC and peridotite initial compositions in the model results.

We modeled trace element effects for several different SC addition and partial melting scenarios. In each case, we model melts as mass-weighted aggregates of modal, incremental-batch partial melting (in increments of 0.1–0.4% melting, depending on the model and integrated extent of melting) of a mixed SC peridotite source with 55% olivine, 30% orthopyroxene, 10% clinopyroxene, 2.5% garnet, and 2.5% spinel. Modeling the melting as non-modal, pure batch, or pure fractional melting does not strongly affect the results for the elements we examined. Due to uncertainties in the depth of subarc mantle melting we assumed equal proportions of garnet and spinel in the peridotite; changing the source to either all garnet or spinel does not significantly affect these results. Distribution coefficients for all elements were taken from Borg et al. (1997), and references therein.

Figure 6 illustrates the three different end-member scenarios of partial melting of SC peridotite mixtures, for which we modeled the trace element effects on melts. The first scenario (Fig. 6A) assumes no correlation between the amount of SC added to the peridotite and the degree of melting. We modeled the trace element effects of this scenario as progressive melting of individual mixed peridotite-SC (metasomatized) sources, with either 0, 1.5, or 5% SC.

The second scenario (Fig. 6B) considered is one in which the degree of melting (F) of the peridotite is a linear function of the amount of SC added to the peridotite. The theoretical basis for a correlation between SC and F is well established. It is based on numerous experimental and theoretical studies (e.g., Hirose and Kawamoto 1995; Gaetani and Grove 1998; Hirschmann et al. 1999) showing that addition of a volatile- and/or alkali-rich component to mantle peridotite lowers the solidus temperature of the peridotite, causing, or increasing the extent of peridotite partial melting. These studies also show that peridotite temperature has a strong influence on the slope of the SC-F correlation: hotter mantle melts to a larger degree per increment of SC metasomatism (higher dF/dSC) than cooler mantle (Fig. 6B). Under isothermal conditions

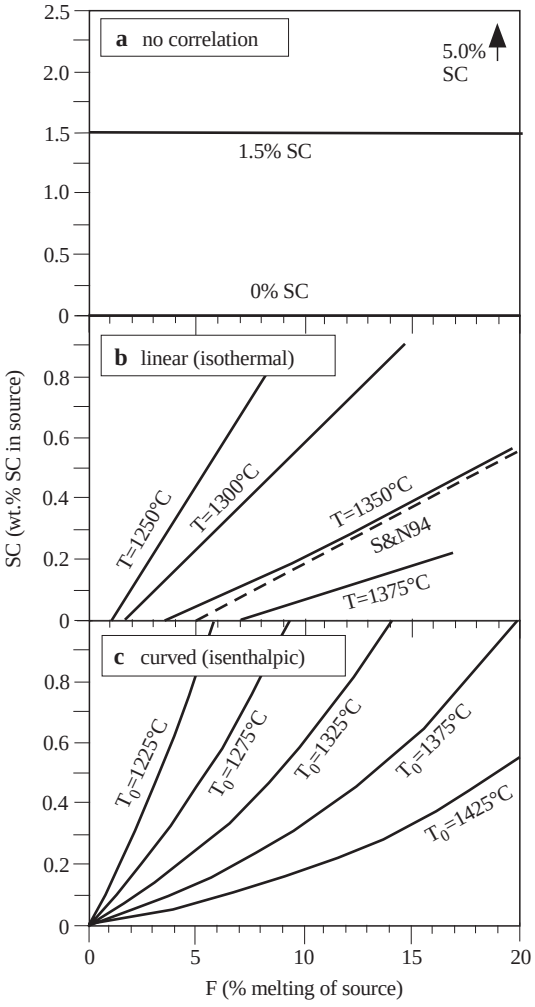

Fig. 6 Three potential relationships between extent of subduction component (*SC*) metasomatism of the peridotite source, and melting (*F*) of the mixed peridotite-SC source. **A** No relationship between amount of SC added to peridotite and F of mixed-source melting (i.e., progressive melting of individual, variably metasomatized sources). We evaluated the trace element predictions of this scenario for three separate sources with 0, 1.5, and 5% SC. **B** Linear correlation between SC and F. SC-F trends are taken from Hirschmann et al. (1999) and represent isothermal flux-melting trends for peridotite of different temperatures at 1.0 GPa, as a result of progressive H_2O added to the peridotite (SC is assumed to comprise 44% H_2O, e.g., Stolper and Newman 1994). Hotter mantle melts to a larger degree per increment of SC metasomatism than colder mantle. *Dashed line labeled S&N94* is flux melting trend calculated from compositions of Mariana back-arc lavas by Stolper and Newman. **C** Curved SC-F correlations ($d^2F/dSC^2 < 1$). As noted by Hirschmann et al. (1999) such curved SC-F trends are predicted by isenthalpic flux melting, in which peridotite temperature decreases with progressive SC metasomatism and melting. Trends in this model are assumed to pass through the origin (some SC metasomatism is required to initiate melting), and are calculated by parameterizing dF/dSC as a function of T in the isothermal trends of Hirschmann et al. (1999), and assuming temperature of the peridotite changes with progressive melting as $T = T_0 - F\Delta H_f/C_p$, where T_0 is initial peridotite temperature prior to melting, ΔH_f is latent heat of fusion and C_p is heat capacity

(in which the temperature of the peridotite is held constant regardless of the extent of SC addition or melting), the SC-F correlation will be approximately linear, at least up to melt fractions of about 20%, corresponding to clinopyroxene-out reactions (Hirschmann et al. 1999). Thus, this second class of model can be considered to represent the effects of isothermal flux melting. There is also strong geochemical evidence that linear SC-F correlation approximating isothermal flux melting functions (Hirschmann et al. 1999; Gaetani and Grove 1998) can explain trace element variations of arc related magma suites (Stolper and Newman 1994). Using the isothermal flux melting MELTS models of Hirschmann et al. (1999), which assumes an SC of 45% H_2O, trace element effects of isothermal flux melting of three different peridotite temperatures (1225, 1275, and 1375 °C) have been modeled. We calculate dF/dSC for each temperature by approximately parameterizing Hirschmann et al.'s isothermal flux melting calculations as:

$$\frac{dF}{dSC} = 3 \times 10^{-6} e^{0.012T} \quad (1)$$

The third melting model we examined assumes that F and SC are non-linearly correlated, specifically that $d^2F/dSC^2 < 1$, or melting productivity decreases as SC and F increase (Fig. 6C). This scenario is similar to isothermal flux melting because larger amounts of SC cause more extensive melting, and higher initial peridotite temperature causes higher dF/dSC. The strong curvature of the SC-F trends, however, is predicted for the case of isenthalpic (rather than isothermal) flux melting, due to the fact that heat consumed by progressive melting decreases the temperature of the peridotite, thus decreasing dF/dSC ratios with increasing F and SC (Hirschmann et al. 1999). We have modeled the trace element effects of isenthalpic flux melting for three cases with different initial peridotite temperatures (1225, 1275, and 1375 °C, Fig. 6C). Our flux melting equations are derived by using the temperature dependence of dF/dSC from Hirschmann et al.'s models [i.e., Eq. (1)], and then assuming that with progressive melting, peridotite temperature decreases as a function of F, latent heat of fusion (ΔH_f) and heat capacity (C_p), assumed to be 753 J/g, and 1.3 J/g K, respectively (Hess 1992; Langmuir et al. 1992), as:

$$T = T_0 - F\frac{\Delta H_f}{C_p} \quad (2)$$

Substituting (2) into (1) yields:

$$\frac{dF}{dSC} = 3 \times 10^{-6} e^{0.012\left(T_0 - F\frac{\Delta H_f}{C_p}\right)} \quad (3)$$

We apply this equation iteratively to progressively melt a mixed peridotite-SC source as a function of SC added (in 0.01 wt% increments), correcting the residual trace element concentrations after each increment of melting, adding a new increment of SC, and aggregating the melt produced up to 30% melting.

In both the isothermal and isenthalpic models, we assume that F = 0 at 0% SC added to the peridotite at any temperature, in contrast to the Hirschmann et al. models

(Fig. 6B) in which at 1.0 GPa, peridotite at any temperature over about 1250 °C has >1% melt present. Our assumption is equivalent to an onset of melting requiring an addition of a finite mass of SC, rather than a peridotite source with a pre-existing melt fraction >0%. This is overly simplistic in detail, but changing the model to assume a pre-SC-flux melt fraction does not affect the important results of our modeling, which are caused by the variations in slopes with temperature and melt fraction. Additionally, the 0% pre-SC-flux melt fraction condition could be considered to suggest that hotter mantle sources are present at higher pressures (assuming that pressure does not play an important role in the dF/dSC curves, which is difficult to ascertain from existing models).

Finally, we also examined the effects of different compositions of peridotite and SC on the trace element predictions of isenthalpic flux melting. In these examples, we use a strongly incompatible element depleted (MORB source) peridotite, and both SC compositions presented in Table 4.

Model results

Figure 7 shows fields of Cascade basalt compositions with respect to LILE and HFSE contents (the fields encompass the same data shown in Fig. 4). It also shows the predictions of the first two melting model scenarios: (1) progressive melting of individual metastomatized sources, and (2) isothermal flux melting. Several important conclusions regarding the relative shapes of the melting trends and data fields can be easily seen with these plots, and the overall results of these examples can be generalized over a wide range of concentrations and ratios of other trace elements.

Partial melting of individual mantle sources that have been metasomatized by different amounts of SC (scenario illustrated in Fig. 6A) predicts a series of positively correlated, slightly concave upward trends (dashed lines) in Fig. 7. Trends corresponding to melting of mantle sources with very small SC contributions (0 to <0.2%) adequately reproduce variations in some OIB-like suites (e.g., Dalles Lakes and Simcoe, Figs. 4, 7). Trends corresponding to melting of mantle sources with very large SC contributions (>2%) also appear to produce melts with CAB compositions. However, trends corresponding to melting of sources with intermediate SC contributions (e.g., 0.5–2%) predict compositions that are intermediate between the observed CAB and OIB fields, where no samples are observed (Fig. 7). If trace element differences between CAB and OIB-like magmas were simply a matter of degree of SC metasomatism of each mantle source, then a broad swath of compositions corresponding to a fan of positively correlated melting trends would be expected, not the clearly distinct and divergent CAB-OIB fields (Figs. 4, 7). Simply varying the amount of SC in each mantle source (without correlation be-

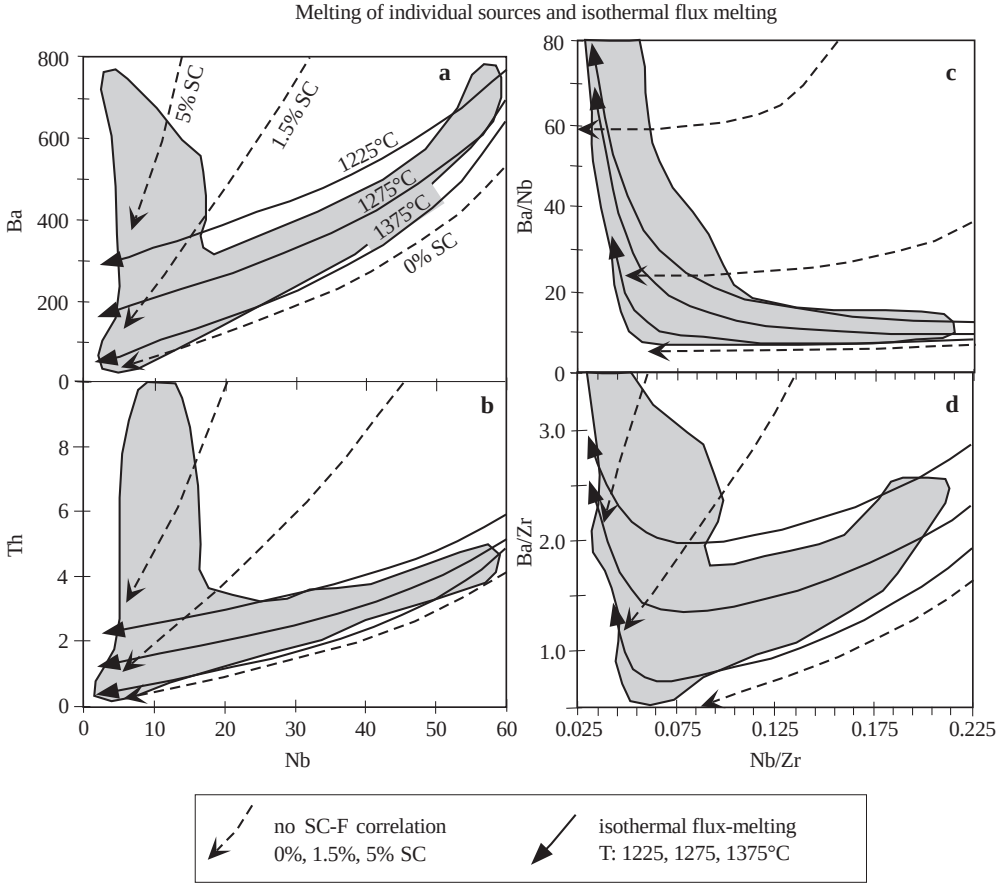

Fig. 7 Fields of data shown in Fig. 4, with model partial melting trends of the SC-F scenarios shown in Fig. 6A and B (progressive melting of individual sources, and isothermal flux melting). All partial melting trends increase in melt fraction from right to left, and are shown for up to 30% integrated melting. *Arrows* point in directions of increasing degree of partial melting. *Dashed black lines* are progressive melting of individual sources metasomatized by either 0, 1.5, or 5% SC (Fig. 6A). *Solid black lines* are melting trends for isothermal SC-F flux-melting (Fig. 6B), and are shown for peridotite temperatures of 1225, 1275, and 1375 °C (colder mantle has higher LILE and LILE/HFSE at a given HFSE than hotter mantle). Neither melting of individual, variably metasomatized sources nor isothermal flux melting reproduce the distinct and divergent CAB and OIB fields in all plots

tween F and SC) cannot explain the CAB-OIB distinction.

Trace element predictions of linear SC-F correlation simulating isothermal flux melting (e.g., the scenario illustrated in Fig. 6B) predict partial melting trends (solid lines in Fig. 7) that reproduce the shape of the data fields with respect to some trace element ratios (Fig. 7). However, these models do not predict the strong divergence of CAB and OIB-like magma compositions in trace element concentration space (Fig. 7), and cannot produce the most extreme CAB magmas with the lowest HFSE and highest LILE. Isothermal flux melting can only explain strongly CAB-like compositions with both low HFSE and high LILE by melting (about 15–25%) extremely cold mantle ($T < 1175$ °C in this model). Lower extents of melting (5–10%) of such cold mantle also predicts compositions intermediate between CAB and OIB-like magmas, where no samples are observed (Figs. 4, 7). Varying the peridotite and SC compositions within reasonable limits (e.g., Borg et al. 1997 MORB to OIB compositions) also does not produce a good fit between the isothermal flux melting trends and the CAB-OIB fields. We conclude that no simple isothermal flux melting model predicts the strongly diverging and distinct CAB and OIB-like fields.

Trace element predictions of isenthalpic flux melting (scenarios illustrated in Fig. 6C) reproduce many features of the distinct and divergent CAB and OIB-like fields (Fig. 8). As observed in previous models, low degree (approximately <8%) partial melts have well correlated LILE and HFSE concentrations, and as both SC and F increase, concentrations of both LILE and HFSE decrease. In the isenthalpic flux melting models, however, as F increases LILE concentrations reach a minimum and then increase, while HFSE concentrations continue to decrease or remain constant in progressively higher degree melts. This transition occurs at about 10% melting for an initial peridotite temperature of 1225 °C, and about 20% for 1375 °C (Fig. 8). This decoupling of LILE and HFSE concentrations at high degrees of melting occurs because SC-source metasomatism begins to have a large effect on LILE melt concentrations at high degrees of melting (10–20%), whereas HFSE concentrations are not significantly affected by SC metasomatism. This decoupling means that high F melts of relatively cold peridotite develop high LILE/HFSE, and partial melting trends are V-shaped or hyperbolic and diverge near the origin, similar to the distinct divergence of the Cascade CAB and OIB-like fields (Fig. 8). The shift from decreasing to increasing LILE concentrations with increasing F is more pronounced for colder peridotite because of the lower dF/dSC of colder mantle and thus larger SC contribution at a given F. Hotter mantle shows less of a LILE-HFSE divergence because SC addition produces a larger increase in F, thereby diluting LILE concentrations in resulting melts.

In the isenthalpic flux-melting model, low degree melts (approximately <10%) are OIB-like regardless of initial peridotite temperature, but if the initial temperature is lower than about 1250 °C (i.e., lower dF/dSC, or a lower degree of melting per increment of SC metasomatism), melts produced by degrees of melting greater than about 10–15% show CAB trace-element signatures. Higher initial mantle temperature (i.e., higher dF/dSC,

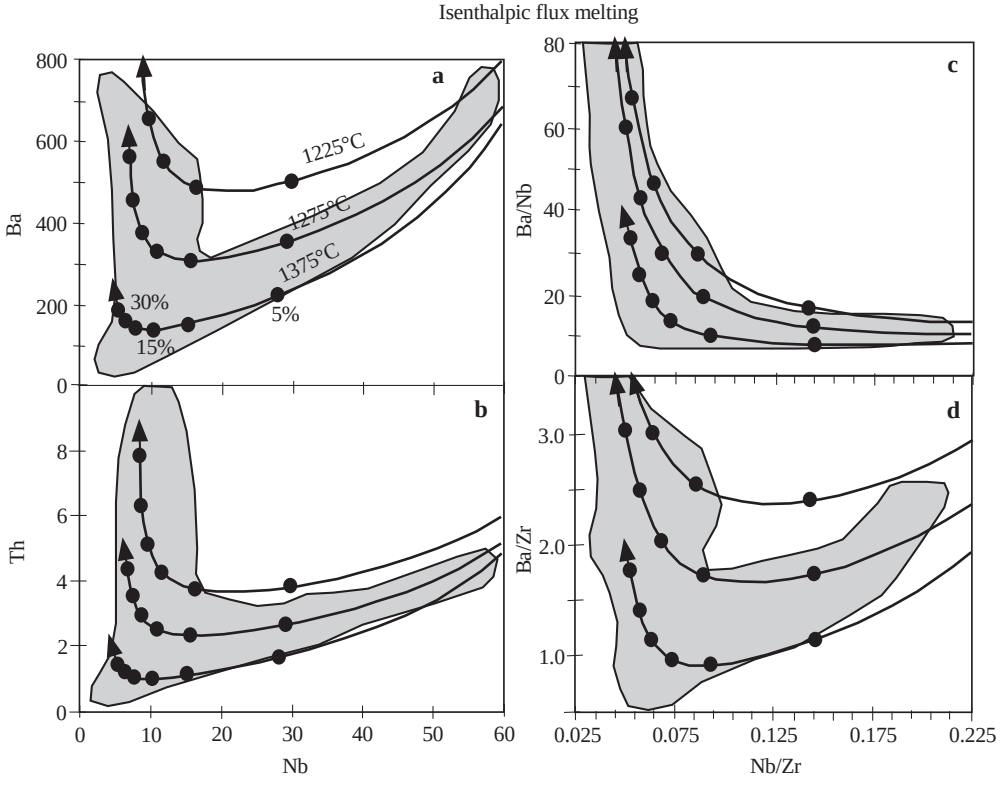

Fig. 8a–d Fields of data shown in Fig. 4, with model partial melting trends of isenthalpic flux melting (scenario shown in Fig. 6C) of peridotite with initial temperatures of 1225, 1275, and 1375 °C. All partial melting trends increase in melt fraction from right to left, and are shown for up to 30% integrated melting. *Arrows* point in directions of increasing degree of partial melting; *circles* are 5% integrated melting intervals. Isenthalpic flux melting trends reproduce most features of the CAB-OIB distinction, and suggest that CAB signatures can be explained as the result of high degrees of melting (which dilutes incompatible elements), caused by high extents of SC metasomatism (which enriches LILE but not HFSE in resulting melts)

or a higher degree of melting per increment of SC metasomatism) shifts the trend towards the origin, in which case even highly SC-metasomatized sources cannot produce significantly LILE-enriched melts because of the higher degree of melting accompanying SC metasomatism (Fig. 8). This may indicate that magmas with CAB trace-element signatures can only be derived from melting of mantle regions with relatively low initial temperatures.

Effect of peridotite and SC compositions on isenthalpic-flux melting trends

Figure 9 illustrates the influence of source peridotite and SC compositions on the trace element predictions of isenthalpic flux-melting. In all cases, including the results in Fig. 8, trace-element trends record a shift from peridotite dominated to SC-dominated compositions, with progressive partial melting. The trends begin with well-correlated concentrations of LILE and HFSE in low degree partial melts that decrease with progressive melting. With higher degrees of SC metasomatism and melting, and independent of the initial peridotite composition, the trends change direction, heading towards the SC bulk composition. Compositional variation of the peridotite and SC sources can therefore have a large effect on trace element trends of isenthalpic flux melting.

Figure 9A shows Ba and Nb concentrations in flux melts using the same SC composition, but the slightly more Ba-enriched and Nb-depleted (Table 4) OIB-source peridotite composition of Borg et al. (1997), as in Fig. 8. The only significant difference between Figs. 8 and 9A is the lower Nb concentrations in the initial low degree partial melts in Fig. 9A. This suggests that the higher Nb concentrations in our SC composition (Figs. 5, 8) are necessary to produce the Cascade OIB-like lavas. Changing the SC composition in Fig. 9A to that used by Borg et al. (1997) does not change the patterns noticeably.

Figure 9B shows Ba and Nb concentrations of isenthalpic flux-melts using the MORB source peridotite composition of Borg et al (1997; Table 4). All melts in this example have extremely low Nb, reflecting the strong incompatible element depletion of the initial peridotite. Progressive SC metasomatism and melting drive melt compositions to higher Ba concentrations at relatively low and constant Nb, due to the high Ba and low Nb content of the SC. This shows that

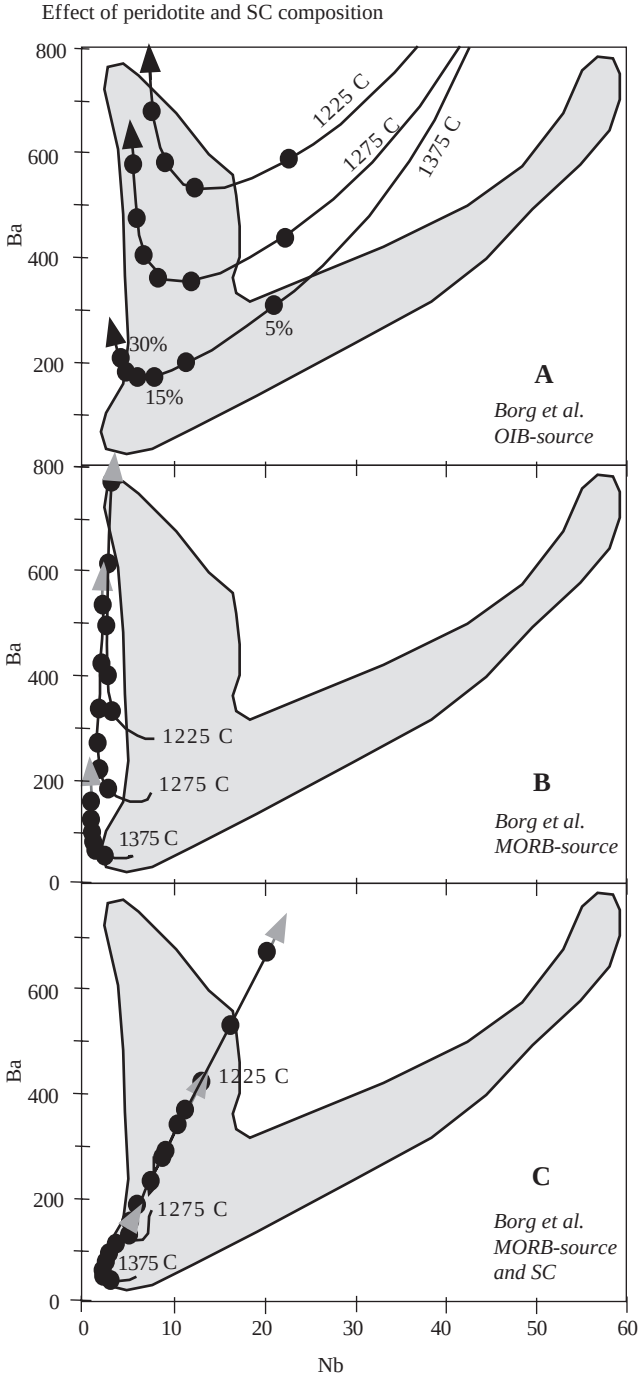

Fig. 9A–C Model partial melting trends of isenthalpic flux melting, using different peridotite and SC compositions. *Arrows* point in directions of increasing degree of partial melting; *circles* are 5% integrated melting intervals. **A** Same SC composition as in Fig. 8, but OIB-source peridotite composition of Borg et al. (1997; Table 4). The lower Nb concentration of Borg et al. (1997) peridotite produces lavas with lower Nb than Cascade OIB-like lavas. Other features of the results are similar to those in Fig. 8. Changing the SC composition to that used by Borg et al. does not noticeably change the trends. **B** Isenthalpic flux melting of peridotite, using same SC as in Fig. 8, but peridotite with a strongly incompatible-element depleted MORB source composition (Fig. 5; Borg et al. 1997). All melts have very low Nb, due to low Nb in both SC and peridotite. Higher degree melts of cold mantle trend towards higher Ba, away from MORB-like compositions and towards, but at lower Nb than, CAB compositions. **C** Flux melting trends assuming SC and MORB-source compositions of Borg et al. (1997). Results are similar to **B**, in that low-degree melts (and higher degree melts of hotter mantle) have compositions similar to MORB-like melts, and higher degree melts of cold mantle trend away from MORB, through CAB compositions, and towards the SC composition

strongly incompatible element-depleted peridotite (i.e., MORB source) cannot be the source of OIB-like lavas.

Using a MORB source peridotite composition, but with the higher Nb SC composition used by Borg et al. (1997; Table 4), shifts the higher degree melts towards higher Nb and Ba. This produces a positive correlation of increasing Ba and Nb concentrations in larger degree melts (Fig. 9C). One important result of these MORB source examples is that in both this and the previous example (Fig. 9B), CAB-like compositions can be produced by relatively large extents of flux melting of relatively cold MORB source peridotite (>about 20% for 1275 °C, and >about 10% for 1225 °C). The positive correlation between Ba and Nb in the CAB field in Fig. 9C is similar to variations observed in the Three Sisters basalts (Fig. 4), suggesting that these lavas could be produced by fluxing of a less Nb-depleted SC composition similar to that used in Borg et al. (1997).

In summary, variations in SC composition, and especially peridotite composition, can have strong influences on the trace element patterns of flux-melting. The peridotite and SC compositions used in the models shown in Fig. 8 can reproduce nearly the entire field of CAB and OIB-like Cascade magmas, as well as MORB-like lavas with low incompatible element concentrations. However, Fig. 9 also shows that CAB and MORB-like magmas (but not OIB-like magmas) can also be produced by flux melting of a strongly incompatible element-depleted MORB source peridotite.

Isenthalpic flux-melting and Cascade basalts

Figure 10 shows trace element compositions of model melts produced by isenthalpic flux melting (using our peridotite and SC compositions; Table 4) that approximate the compositions of DL and TS magmas. The DL sample 96PRDR2 can be modeled as low degree melt (4–5%) of peridotite metasomatized by small amounts of SC (0.2–0.3%). This corresponds to an isenthalpic flux melting trend with an initial peridotite temperature of about 1325 °C (Figs. 6C, 8). In contrast, TS lavas can be modeled as larger degree melts (22%) of peridotite metasomatized by large amounts of SC (4.0%), corresponding to an initial peridotite temperature of 1275 °C. Assuming an SC with 44% H_2O (Stolper and Newman 1994), this would mean that the mantle sources of the DL and TS lavas were fluxed by 0.1 and 1.8% H_2O, corresponding to primary magma compositions with 2.2 and 8.0% H_2O, respectively.

Other studies have suggested similar relative and absolute extents of melting for similar types of arc basalts. Stolper and Newman (1994) concluded that LILE/HFSE, H_2O content, and degree of melting were correlated in Mariana back arc ($F \sim 5$–20%) and arc ($F \sim 15$–35%) lavas. Baker et al. (1994) also found similar results from southern Cascades (Mt. Shasta) lavas, and in combination with experimental evidence suggested that high alumina basalts have low H_2O (essentially anhydrous), and were produced by low extents of melting (6–10%), whereas high MgO basaltic andesites and andesites have high H_2O (3–6%) and were produced by higher degrees of melting (20–30%). In agreement with the interpretations here, the studies of Stolper and Newman (1994) and Baker et al. (1994) suggest that LILE/HFSE, H_2O, and degree of melting are generally correlated in primitive arc magmas, and reflect the flux melting induced correlation between SC addition and degree of melting. This contradicts the interpretations of Conrey et al. (1997) that degree of melting decreases for magmas with progressively higher LILE/HFSE and H_2O (in the order OIB-like basalt, CAB, basaltic andesite, and absarokite). Conrey et al.'s (1997) inferred inverse relationship between LILE/HFSE and degree of melting also requires a special explanation for the strong HFSE depletions in basaltic andesites and absarokites, in the form of residual HFSE-bearing minerals, unusual mantle source, or melt peridotite reaction. In contrast, flux melting, with the

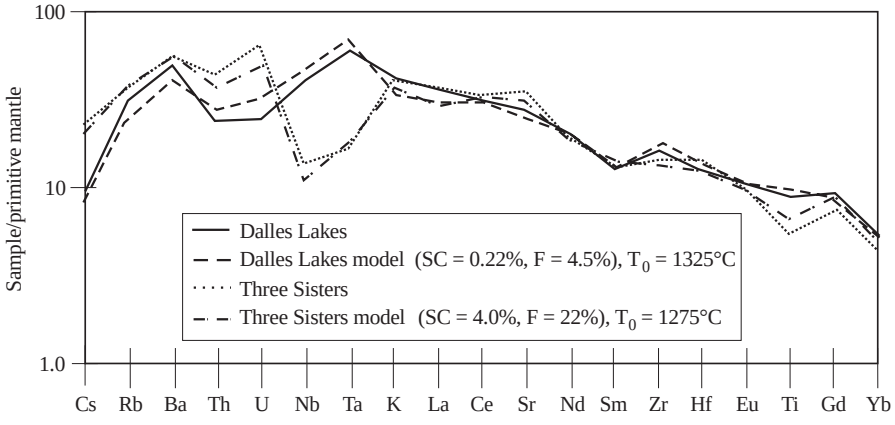

Fig. 10 Trace-element compositions of model melts produced by isenthalpic flux melting, compared with compositions of DL and TS basalts. Assuming our peridotite and SC compositions shown in Fig. 5 and a flux-melting relation of Eq. (3), DL magmas can be adequately modeled by relatively low F and SC, with an initial peridotite source temperature of about 1325 °C, whereas TS magmas can be modeled by relatively high F and SC, with an initial peridotite source temperature of about 1275 °C

main feature of correlated extents of HFSE depletion (by high degrees of melting), and LILE and H_2O enrichment (by SC metasomatism), explains the main compositional features of these diverse types of primitive arc magmas. It should also be noted that especially high LILE/HFSE magmas, such as absarokites, may not require extremely high degrees of melting in any individual melting event. Instead, they may represent moderate degrees of flux melting of peridotite depleted by previous flux melting events, as proposed for the Mariana arc magmas by Stolper and Newman (1994).

The differences in predicted H_2O contents of the primary DL and TS lavas from the isenthalpic flux melting model are consistent with evidence from other studies, but the predicted H_2O content of the TS magma is high relative to estimates for most arc melts. Based on petrologic constraints and comparison to experimental evidence, OIB-like basalts from the Cascades have been estimated to have low to moderate amounts of H_2O (e.g., up to 1%; Conrey et al. 1997). In contrast, on the basis of melt inclusion compositions, petrographic and petrologic estimates, and experimental evidence (Anderson 1974a, b, 1976; Sisson and Grove 1993; Baker et al. 1994), several studies have estimated magmas parental to basaltic andesites and andesites with CAB signatures from Mt. Shasta to contain 3–6.5% H_2O. Other measurements of H_2O contents in mafic melt inclusions in arc basalts and basaltic andesites range widely from nearly anhydrous for high alumina MORB-like basalts, to >6 wt% in some lavas, with typical values of about 2% (e.g., Harris and Anderson 1984; Sisson and Layne 1993; Sobolev and Chaussidon 1996).

The prediction of 8% H_2O for the primary Three Sisters magma is high compared with these measurements. Assuming that this prediction is too high for a primary arc magma, there are a number of possible reasons for this discrepancy. These include: (1) overestimation of the SC H_2O content, (2) decoupling of H_2O from trace elements during SC infiltration, melting, or melt migration, (3) incomplete H_2O extraction from the SC metasomatized source, possibly because of the presence of residual hydrous phases (which may mean amphibole or other hydrous phases are required in trace element models), or (4) a multiple-stage melting process for the TS lavas such that the 22% estimate is an integrated value reflecting more than one SC fluxing and melt depletion event (e.g., Stolper and Newman 1994). In any case, comparing and reconciling H_2O contents and trace element signatures of primary arc magmas is an important issue for the evaluation of flux melting models. The relatively (and probably unrealistically) high H_2O contents implied by this model for strongly CAB lavas such as the Three Sisters basalts may suggest additional complications in the subarc melting process. One possible example is chromatographic effects on the SC or melt (e.g., Stolper and Newman 1994) that may preclude using a single SC composition to model all melts.

Isotope-trace element correlation

Although most isotopic and trace element compositions of primitive arc basalts from southern Washington and northern Oregon are not well correlated, Ba/Nb and $^{87}Sr/^{86}Sr$ do show some correlation (Leeman et al. 1990; Conrey, unpublished data; Fig. 11). By assuming a peridotite $^{87}Sr/^{86}Sr$ of 0.7027, an SC $^{87}Sr/^{86}Sr$ 0.7036–0.7038, and modeling melts as isenthalpic flux melts from peridotite at a range of temperatures between approximately 1225 and 1350 °C, we can reproduce the overall Ba/Nb and $^{87}Sr/^{86}Sr$ correlation (Fig. 11). This is not a unique solution but the correspondence of the isotopic-trace element correlation to the prediction of the flux melting trends supports the proposal of an SC-F correlation, and a dominant role of flux melting in Cascade arc magma genesis.

Origin of the CAB trace-element signature

Our interpretations of a flux melting cause for trace element differences between CAB and OIB-like basalts support previous interpretations of a correlation between fluid fluxing and degree of melting in some continental arc magmas (e.g., Barragan et al. 1998). In addition, our modeling supports previous suggestions (Gill 1981;

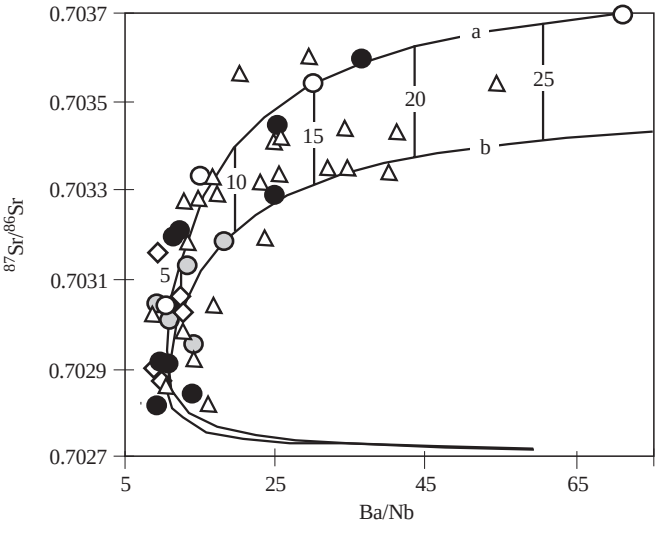

Fig. 11 Ba/Nb and $^{87}Sr/^{86}Sr$ of basalts from Mt. Adams, Mt. St. Helens, Simcoe, and Indian Heaven (data from Leeman et al. 1990; Bacon et al. 1997) and the northern Oregon Cascades (Conrey, unpublished data) with compositions of model melts for isenthalpic flux-melting. Model trends assume our peridotite and SC compositions (Table 4), an initial peridotite temperature of 1275 °C, and peridotite $^{87}Sr/^{86}Sr$ of 0.7027, and SC $^{87}Sr/^{86}Sr$ of 0.7038 (trend *a*) and 0.7036 (trend *b*). Using mantle temperatures from about 1225 to 1375 °C makes little difference in the position of the model trend, although the positions of integrated melt fractions along the trends do change. Three northern Oregon samples with Ba/Nb greater than 75 have been cut off to show detail in the lower Ba/Nb part of the curve, but these three samples have high $^{87}Sr/^{86}Sr$ (0.7035–0.7037) that fall on projections of the melting trends

Woodhead 1989; Stolper and Newman 1994) that the distinctive negative HFSE anomalies and high LILE/HFSE of CAB magmas can be explained simply by large extents of SC metasomatism and large degrees of melting of mixed peridotite-SC source, and do not require special residual Nb- and Ta-rich phases. Alone, high extent of melting produces melts with low incompatible element concentrations, but the correlation (and probably causal relationship between) the extent of SC metasomatism and degree of melting means that as HFSE concentrations decrease due to progressive melting, LILE concentrations are simultaneously enriched in the source and potentially, in the melt. The important question for the origin of the CAB signature is whether dilution by melting or source enrichment by SC metasomatism more strongly influences melt compositions. Two conditions are necessary to produce the high LILE/HFSE characteristic of CAB magmas: low dF/dSC and high F. If dF/dSC is low, LILE enrichment by SC metasomatism overwhelms LILE depletion by melting. If, in addition, the degree of melting is high so that HFSE concentrations are depleted, the resulting magma will have high LILE/HFSE. These effects are most pronounced for high degrees of melting of cold peridotite, and isenthalpic flux melting of such mantle can produce CAB magmas regardless of its initial composition (Figs. 8, 9).

Several different scenarios can lead to OIB- or MORB-like melt compositions instead of CAB. Firstly, if the peridotite is initially cold (low dF/dSC), but the degree of melting is low, then LILE and HFSE concentrations in the melt are not strongly decoupled and magmas do not develop a CAB signature. In this case, if the initial peridotite is not strongly depleted of incompatible elements, the melts are OIB-like (Fig. 8), whereas if the initial peridotite is strongly depleted of incompatible elements, the melts are MORB-like (Fig. 9B, C). Secondly, if the degree of melting is high, but the mantle source is initially hot (high dF/dSC), melting keeps pace with SC metasomatism so that addition of LILE has little effect compared with dilution by melting, and LILE and HFSE concentrations are both low. In this case, if the peridotite is not depleted and the degree of melting is not too high, the melts have an OIB-like composition (Fig. 8), whereas if the peridotite is initially depleted or the degree of melting is high, the melts are MORB-like in composition (Fig. 9B, C). Finally, if the degree of melting is low, but the mantle is initially hot, melts can be either OIB- or MORB-like, depending on the initial peridotite composition (Figs. 8, 9).

The significance of OIB-like magmas in arcs

The observation that many primitive Cascade magmas possess OIB-like, rather than CAB trace element signatures, has led to the suggestion that material from the subducted slab plays little role in Cascade petrogenesis, and that other processes such as shear heating and mantle convection play a more dominant role (e.g., Leeman et al. 1990). The trace element models presented here, however, indicate that OIB-like arc lavas do not necessarily preclude the addition of slab-derived SC to the mantle wedge, or magmatism by flux melting. Lavas with a range of trace element signatures, from CAB to OIB-like (with a distinctive divergence in trace element plots as in Fig. 4), can be simply produced by a single process of SC-induced flux melting of a single mantle source composition over a range of mantle temperatures. It is important to note however, that OIB-like arc basalts cannot be produced from strongly incompatible element-depleted mantle sources (i.e., MORB source mantle) by flux melting, but CAB lavas can.

Other workers (e.g., Márquez et al. 1999) have suggested that in some cases OIB-like magmas in an arc setting indicate the presence of a mantle plume beneath the arc. Our results, however, clearly show that the trace element signatures that typify OIB-like arc lavas can be produced simply by relatively low degrees of a peridotite source that is not strongly depleted of incompatible elements. This could occur by partial melting either in response to SC fluxing or not, but the common association of CAB and OIB-like lavas in arcs suggests that flux melting plays at least some role.

In summary, our results have shown that OIB-like magmas in arcs do not necessarily preclude the addition of slab-derived SC in the mantle wedge, nor do they require special mantle plume activity under an arc. Because CAB trace element signatures require both low dF/dSC and high F, OIB-like (or MORB-like) magmas can be expected and explained in the context of arc melting, in cases where dF/dSC is high, or F is low, or both. In the absence of robust isotopic constraints (such as He isotopes) indicative of plume-like mantle sources, it is simpler to explain OIB-like arc magmas by the same flux melting process and the same peridotite and SC sources that produce CAB magmas. A similar interpretation could be warranted in cases of older volcanic rocks for which the tectonic environments are not clear. Lack of CAB-like trace element signatures (and the presence of OIB- or MORB-like compositions) in ancient lava sequences may not necessarily preclude an arc environment for their formation, especially given that mantle wedge temperatures (and therefore dF/dSC) were probably higher in Precambrian arcs.

Conclusions

The young ages of the DL and Three Sisters basalts (2.2 Ma and 370–400 ka, respectively) show that not all the late Cenozoic to recent volcanism in the central Washington Cascades is associated with large andesitic stratocones and their satellitic vents. The compositions of basalts from these two vents are distinct in several respects. Most importantly, they have strongly contrasting LILE/HFSE that characterize the CAB-OIB distinction for many Cascade lavas, as well as lavas from other arcs. Simple predictions of flux melting of mantle

peridotite can adequately reproduce the strongly divergent trace element compositions of both CAB and OIB-like magmas. Correlation between the amount of subduction-related fluid (SC) added to a peridotite source, and the degree of melting of the source, produces trace element trends that appear to form diverging arrays, not predicted by melting of a continuum of individual sources. The unusual trace element trends of flux melting are due to the depletion of incompatible elements in the melt with increasing degree of melting, and simultaneous enrichment of LILE by SC addition to the source. If both the amount of SC addition and the degree of melting are sufficiently high, magmas will have low HFSE and high LILE, characteristic CAB signatures. This should be the case for large degrees of isenthalpic flux melting of relatively cold mantle. Other situations, such as low degrees of melting or low amounts of SC addition relative to degree of melting, will produce OIB- and MORB-like magmas.

It is likely that the extents of melting and SC metasomatism are often correlated in arc magmatism. Given that SC has large concentrations of many incompatible elements, and as shown here by the complicated trace element trajectories of flux melting, it will be difficult to accurately interpret magmatic compositional variations or determine mantle source compositions without explicitly modeling this correlation. Other types of magmas may also have an origin involving flux melting, especially those not obviously related to mantle upwelling beneath ridges or hotspots. In such cases, mantle metasomatism that induces melting may be analogous to SC addition in arcs, and the possible link between mantle source composition and degree of melting should be considered.

Acknowledgements We thank Grant Newport and Jeannie Hunt of Weyerhauser for access to and navigational help in the Three Sisters region. We appreciate constructive reviews from Jim Luhr and Rick Conrey, and comments on an early version of this paper by Gwyneth Jones and Bruce Nelson. We also appreciate helpful discussions with John Eiler, Marc Hirschmann, and Tom Sisson. Thanks to Ken Farley for support for Reiners' moonlighting on this project at Caltech.

References

Anderson AT (1974a) Evidence for a picritic, volatile-rich magma beneath Mt. Shasta, California. J Petrol 15: 243–267

Anderson AT (1974b) Chlorine, sulfur, and water in magmas and oceans. Geol Soc Am Bull 85: 1492–1585

Anderson AT (1976) Magma mixing: Petrological process and volcanological tool. J Volcanol Geothermal Res 1: 3–33

Ayers JC, Dittmer SK, Layne GD (1997) Partitioning of elements between peridotite and H_2O at 2.0–3.0 GPa and 900–1100 °C, and application to models of subduction zone processes. Earth Planet Sci Lett 150: 381–398

Bacon CR, Bruggman PE, Christiansen RL, Clynne MA, Donnelly-Nolan JM, Hildreth W (1997) Primitive magmas at five Cascade volcanic fields: melts from hot, heterogeneous sub-arc mantle. Can Mineral 35: 397–423

Baker MB, Grove TL, Price R (1994) Primitive basalts and andesites from the Mt. Shasta region, N. California: products of varying melt fraction and water content. Contrib Mineral Petrol 118: 111–129

Barragan R, Geist D, Hall M, Larson P, Kurz M (1998) Subduction controls on the compositions of lavas from the Ecuadorian Andes. Earth Planet Sci Lett 154: 153–166

Borg LE, Clynne MA, Bullen TD (1997) The variable role of slab-derived fluids in the generation of a suite of primitive calc-alkaline lavas from the southernmost Cascades, California. Can Mineral 35: 425–452

Conrey RM, Sherrod DR, Hooper PR, Swanson DA (1997) Diverse primitive magmas in the Cascade arc, northern Oregon and southern Washington. Can Mineral 35: 367–396

Dunn T, Stolper EM, Baker MB (1993) Partial melting of an amphibole-bearing lherzolite at 1.5 GPa (Abstr). Geol Soc Am Abstr with Prog 25: 213

Fischer JF (1970) The geology of the White River-Carbon Ridge area, Cedar Lake quadrangle, Cascade Mountains, Washington. PhD Thesis, University of California, Santa Barbara

Gaetani GA, Grove TL (1998) The influence of water on melting of mantle peridotite. Contrib Mineral Petrol 131: 323–346

Gill JB (1981) Orogenic andesites and plate tectonics. Springer, Berlin Heidelberg New York, 358 pp

Hammond PE (1980) Reconnaissance geologic map (1:125,000) and cross sections of southern Washington Cascade Range, latitude 45°30′N–47°15′N, longitude 120°45′–122°22.5′W: Portland State University, Department of Earth Sciences, p 31, 2 pl

Hammond PE (1998) Tertiary andesitic lava-flow complexes (stratovolcanoes) in the southern Cascade Range of Washington – observations on tectonic processes within the Cascade arc. Wash Geol 26: 20–30

Harris DM, Anderson AT Jr (1984) Volatiles H_2O, CO_2, and Cl in a subduction related basalt. Contrib Mineral Petrol 87: 120–128

Hartman DA (1973) Geology and low-grade metamorphism of the Greenwater River area, central Cascade Range, Washington. PhD Thesis, University of Washington, Seattle

Hawkesworth CJ, Gallagher K, Hergt JM, McDermott F (1993) Mantle and slab contributions in arc magmas. Annu Rev Earth Planet Sci 21: 175–204

Hawkesworth CJ, Gallagher K, Hergt JM, McDermott F (1994) Destructive plate margin magmatism: geochemistry and melt generation. Lithos 33: 169–188

Hess PC (1992) Phase equilibria constraints on the origin of ocean floor basalts. In: Phipps Morgan J, Blackman DK, Sinton JM (eds) Mantle flow and melt generation at mid-ocean ridges. Am Geophy Union Geophys Monogr 71: 67–102

Hirschmann MM, Asimow PD, Ghiorso MS, Stolper EM (1999) Calculation of peridotite partial melting from thermodynamic models of minerals and melts. III. Controls on isobaric melt production and the effect of water on melt production. J Petrol 40: 831–851

Hirose K, Kawamoto T (1995) Hydrous partial melting of lherzolite at 1GPa – the effect of H_2O on the genesis of basaltic magmas. Earth Planet Sci Lett 133: 463–473

Ionov DA, Hofmann AW (1995) Nb-Ta-rich mantle amphiboles and micas: Implications for subduction-related metasomatic trace element fractionations. Earth Planet Sci Lett 131: 341–356

Langmuir CH, Klein EM, Plank T (1992) Petrological systematics of mid-ocean ridge basalts: constraints on melt generation beneath ocean ridges. In: Phipps Morgan J, Blackman DK, Sinton JM (eds) Mantle flow and melt generation at mid-ocean ridges. Am Geophys Union Geophys Monogr 71: 183–280

Lanphere MA, Sisson TW (1995) K-Ar ages of Mount Rainier volcanics. EOS Trans Am Geophy Union 76: 651

Leeman WP, Smith DR, Hildreth W, Palacz Z, Roges N (1990) Compositional diversity of late Cenozoic basalts in a transect across the southern Washington Cascades: implications for subduction zone magmatism. J Geophys Res 95: 19561–19582

Luedke RG, Smith RL (1982) Map (1:1,000,000) showing the distribution, composition, and age of late Cenozoic volcanic centers in Oregon and Washington. USGS Map I-1091-D

Luhr JF (1997) Extensional tectonics and the diverse primitive volcanic rocks in the Western Mexican volcanic belt. Can Mineral 35: 473–500

Luhr JF, Allan JF, Carmichael ISE, Nelson SA, Hasenaka T (1989) Primitive calc-alkaline and alkaline rock types from the western Mexican volcanic belt. J Geophys Res 94: 4515–4530

Márquez A, Oyarzun R, Doblas M, Verma SP (1999) Alkalic (ocean-island basalt type) and calc-alkalic volcanism in the Mexican volcanic belt: a case for plume-related magmatism and propagating rifting at an active margin? Geology 27: 51–54

McKenna JM (1994) Geochemistry and petrology of Mount Rainier magmas: petrogenesis at an arc-related stratovolcano with multiple vents. MS Thesis, University of Washington, Seattle

Menner AV, Dunn T (1995) Amphibole and phlogopite stability in an initially amphibole-bearing spinel peridotite under water-saturated conditions; 1 to 2.5 GPa (Abstr). EOS Trans Am Geophys Union 76 Suppl 46: 697

Miyashiro A (1978) Nature of alkalic volcanic rock series. Contrib Mineral Petrol 66: 91–104

Niida K, Green DH (1999) Stability and chemical composition of pargasitic amphibole in MORB pyrolite under upper mantle conditions. Contrib Mineral Petrol 135: 18–40

Sen C, Dunn T (1995) Experimental modal metasomatism of a spinel lherzolite and the production of amphibole-bearing peridotite. Contrib Mineral Petrol 119: 422–432

Sisson TW, Grove TL (1993) Temperature and H_2O contents of low-MgO high-alumina basalts. Contrib Mineral Petrol 113: 167–184

Sisson TW, Lanphere MA (1997) The growth of Mount Rainier volcano, Cascade arc, USA. IAVCEI General Assembly, Puerto Vallarta, Mexico, p 5

Sisson TW, Layne GD (1993) H_2O in basalt and basaltic andesite glass inclusions from four subduction-related volcanoes. Earth Planet Sci Lett 117: 619–635

Sobolev AV, Chaussidon M (1996) H_2O concentrations in primary melts from supra-subduction zones and mid-ocean ridges: implications for H_2O storage and recycling in the mantle. Earth Planet Sci Lett 137: 45–55

Stolper E, Newman S (1994) The role of water in the petrogenesis of Mariana trough magmas. Earth Planet Sci Lett 121: 293–325

Sun M, Kerrich R (1995) Rare earth element and high field strength element characteristics of whole rocks and mineral separates of ultramafic nodules in Cenozoic volcanic vents of southeastern British Columbia, Canada. Geochim Cosmochim Acta 59: 4863–4879

Sun SS, McDonough WF (1989) Chemical and isotopic systematics of oceanic basalts: implications for mantle composition and processes. In: Saunders AD, Norry MJ (eds) Magmatism in the ocean basins. Blackwell Scientific, London, pp 313–345

Tatsumi Y, Hamilton DL, Nesbitt RW (1986) Chemical characteristics of fluid phase released from a subducted lithosphere and origin of arc magmas: evidence from high-pressure experiments and natural rocks. J Volcanol Geotherm Res 29: 293–309

Woodhead JD (1989) Geochemistry of the Mariana arc (western Pacific): source composition and processes. Chem Geol 76: 1–24